Engineering Optimization

ISSN: (Print) (Online) Journal homepage: https://www.tandfonline.com/loi/geno20

Development of a joint distance constraint for optimized topology and optimized connection for multiple components

Jun Hwan Kim, Young Hun Choi & Gil Ho Yoon

To cite this article: Jun Hwan Kim, Young Hun Choi & Gil Ho Yoon (2023) Development of a joint distance constraint for optimized topology and optimized connection for multiple components, Engineering Optimization, 55:9, 1456-1476, DOI: 10.1080/0305215X.2022.2089879

To link to this article: https://doi.org/10.1080/0305215X.2022.2089879

ENGINEERING OPTIMIZATION
2023, VOL. 55, NO. 9, 1456–1476
https://doi.org/10.1080/0305215X.2022.2089879

Taylor & Francis
Taylor & Francis Group

RESEARCH ARTICLE

Development of a joint distance constraint for optimized topology and optimized connection for multiple components

Jun Hwan Kim, Young Hun Choi and Gil Ho Yoon

School of Mechanical Engineering, Hanyang University, Seoul, South Korea

ABSTRACT

This article develops a new topology optimization scheme for finding optimized joints for multiple components. As the optimized topologies for each component are determined by several structural conditions, simultaneously optimizing the joint location as well as the optimized topology is regarded as one of the difficult problems. Because joint connections are normally defined at nodes, inevitably the optimized locations of joints are mesh dependent. To contribute to these research topics, this research presents a new method for controlling the optimized location of joints. In particular, a joint dispersal constraint is developed in order to control the number and optimized locations of optimized joints. With the developed scheme, it is possible to find optimized joints as well as optimized topology while maintaining a minimum distance between all joints. To show the effectiveness of the present optimization scheme, several numerical optimization problems are solved.

ARTICLE HISTORY
Received 19 July 2021
Accepted 12 February 2022

KEYWORDS
Topology optimization; multi-component; joint location; joint distance

1. Introduction

A new topology optimization method for designing optimized joints for multiple components is developed in the present study. One of the important subjects in computational mechanics is to consider the optimized connections as well as the optimized topologies for multiple components. Since several structural conditions such as loading, boundary and material properties can strongly influence the optimized topologies, the optimization of joint location simultaneously with topologies is a difficult design problem. Some relevant studies normally implement pseudo rigid springs making the mechanical displacements at the nodes the same. Because the joint connections are normally defined at nodes, the optimized topological layouts will be different depending on the mesh size as shown in Figure 9 in Example 1. By refining the mesh, different layouts and the associated joints are observed. The optimized locations of joints are inevitably affected by mesh dependency. In the case of friction stir spot welding, as shown in Figure 1(a), maintaining the distance between each weld is important (Rajadhyaksha 2016). To contribute to this research topic, this article presents a new method to control the optimized location of joints. In particular, the joint dispersal (JD) constraint is developed in order to control the number and optimized location of optimized joints. In the present study, the JD constraint is presented to control the number and optimal locations of optimal joints maintaining the maximum distance between them.

After the development of the structural topology optimization scheme, some relevant studies have been proposed for optimized joint design as shown in Figure 1(b). In Chickermane and

CONTACT Gilho Yoon ghy@hanyang.ac.kr, gilho.yoon@gmail.com

This article has been corrected with minor changes. These changes do not impact the academic content of the article.

Supplemental data for this article can be accessed here. https://doi.org/10.1080/0305215X.2022.2089879

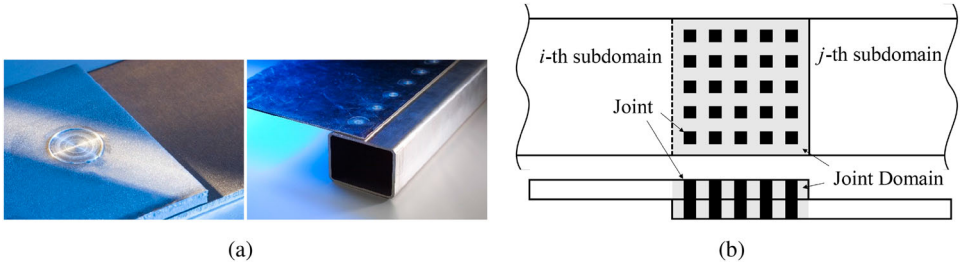

Figure 1. (a) Friction stir spot welding maintaining the distance between welds (Courtesy of RIFTEC GmbH via https://www.riftec.de/). (b) Schematic multi-component model with joint domain.

Gea (1996), a multi-component topology optimization scheme with optimization of the joint location was proposed. These authors also considered the optimization of welding locations with the employment of spring elements. In Jiang and Chirehdast (1996), Qing Li, Steven, and Xie (2001) and Thomas, Li, and Steven (2020), the importance of the locations and patterns of the connections in structural optimization was investigated and discussed. In Qing Li, Steven, and Xie (2001), the Evolutionary Structural Optimization (ESO) method was employed for joint optimization. In Thomas, Li, and Steven (2020), the Bi-Directional Evolutionary Structural Optimization (BESO) method was applied for optimized topology and joint configuration. In Ambrozkiewicz and Kriegesmann (2021), a spring element was employed to model welding and bolts. The initial number of joints is predefined and the location of circular or ring spring patterns are considered during optimization procedure. Circular or ring spring patterns are considered. A minimum distance constraint is also provided to ensure a minimum clearance of the fastener. In Yildiz and Saitou (2011), Guirguis *et al.* (2015) and Woischwill and Kim (2018), interface modelling between components with quad and beam elements was proposed. In Yuqing Zhou and Saitou (2018), the number of multiple components was controlled. In Yuqing Zhou, Nomura, and Saitou (2018), an anisotropic composite was considered in structural optimization. In Kang, Wang, and Wang (2016) and Wang *et al.* (2018), the level-set method and the MMC approach were applied for structural optimization with multiple components. In the concept of the level-set method, interference between components is constrained. In Zhu *et al.* (2015), the node mismatching issue was efficiently resolved by the Multi-Point Constraint (MPC). In Zhu, Zhang, and Xia (2016), the die casting direction was also imposed for structural optimization. In Zhu, Zhang, and Beckers (2009) and Zhu and Zhang (2010), an integrated layout design process dealing with the topology and the support layout was proposed. In Zhu, Zhang, and Beckers (2009), Zhu and Zhang (2010), Zhu *et al.* (2008) and Zhang *et al.* (2012), a remeshing scheme was employed for the structural optimization of multiple components. In Zhang *et al.* (2012), a structural optimization scheme with static load and random excitation was developed. A self-connected material interpolation with multiple dissimilar microstructures was proposed to handle multi-domain topology optimization in Luo, Hu, and Liu (2021). Besides research regarding multiple components, the multimaterial optimization scheme is also relevant because the determination and choice of the proper and optimized material are important. In Liu, Shi, and Kang (2020) and Liu, Luo, and Kang (2016), the consideration of multiple components was carried out with the help of the level-set method. In Liu and Kang (2018), a remeshing scheme was considered along the interface. In Kim *et al.* (2020), tension/compression and adhesive characteristics were modelled with single design variables. In addition, several studies with multiple components and manufacturing constraints exist (Hao Zhou *et al.* 2019; Langelaar 2019; Hur *et al.* 2019; Quhao Li *et al.* 2016). As the consideration of the multiple components in structural topology optimization is important, this research also develops a new approach for the joint design for multiple components.

The present study also considers structural optimization for joints among multiple components. Spring elements are used to model the joint and the lengths of the joints are set to zero to ensure

the connected component condition. From an engineering point of view, sufficiently strong stiffness values are assigned for the stiffness values of the joints. During the optimization process, it is recognized that the aggregation of the joints without any restriction in a certain area becomes a serious issue as unwanted redundant constraints can occur. To remove and control this, it is possible to calculate and constrain the distances between joints (Ambrozkiewicz and Kriegesmann 2021). In the present approach, alternatively, the number of joints in a specific area is calculated and constrained with the p-norm formulation. One joint design variable is assigned to the springs connected to the nodes of each element in order to remove rigid body rotation, *i.e.* one design variable for four springs in the case of a four-node plane element. To calculate the joint distance, the design domain or the joint domain is divided into several joint subdomains and the maximum number of joints is constrained. The stiffness interpolation method in Yoon *et al.* (2008) is considered in order to increase the convergence of the joint design variables. To show the validity of the present approach, several two-dimensional problems, shell problems and three-dimensional problems are considered.

The remainder of this article is arranged as follows: Section 2 provides an overview of the topology optimization formulation with multi-components and the joint model. The optimization formulation with the joint modelling is presented with the Joint Dispersal (JD) constraint to control the location of joints. Section 3 presents several numerical examples in order to validate the present approach. The conclusions and findings are summarized in Section 4.

2. Topology optimization formulation for multiple components and joint modelling

This section develops the new joint modelling method and the minimum joint distance constraint in topology optimization for multiple components. A new topological design method simultaneously optimizing the topology for multiple components and joints connecting between multiple components is developed here.

2.1. Topology optimization formulation with joint constraints

Mathematically, the control and region determination of joints can be described as constraints in the topology optimization framework. These constraints called joint constraints in the present study. Before presenting the joint constraints, the analysis theory and optimization formulation are briefly summarized here. The topology optimization problem minimizing the compliance subject to the volume constraint and the joint constraint is formulated based on the Solid Isotropic Material with Penalization (SIMP) interpolation function and polynomial interpolation function in Yoon *et al.* (2008). The finite element formulation is employed to solve the equilibrium equation in the analysis domain Ω as follows:

$$\nabla \cdot \boldsymbol{\sigma}(\mathbf{u}) + \mathbf{b} = \mathbf{0} \text{ in } \Omega, \quad \boldsymbol{\sigma} = \mathbf{C}\boldsymbol{\varepsilon}, \tag{1}$$

where the stress tensor, the displacement field vector and the body force are denoted by $\boldsymbol{\sigma}$, $\mathbf{u}$ and $\mathbf{b}$, respectively. The body force term is neglected in the present study. The strain tensor and the constitutive matrix are denoted by $\boldsymbol{\varepsilon}$ and $\mathbf{C}$, respectively.

In Figure 2, the analysis domain Ω is divided into the m-subdomains Ω^i $(i = 1, 2, \ldots, m)$, where the number of the subdomain is denoted by m. The overlap region between the i-th and the j-th subdomains is defined by the joint domain, $\Omega^{i,j}$, as follows:

$$\Omega = \Omega^1 \cup \cdots \Omega^i \cup \Omega^j \cdots \cup \Omega^m, \quad \Omega^i \cap \Omega^j = \Omega^{i,j}. \tag{2}$$

Note that the joint domain $\Omega^{i,j}$ is the overlap region between the i-th and the j-th subdomains and cannot be an empty set. The joint subdomain $\Omega^{i,j,k}$ $(k = 1, 2, \ldots, m^{i,j})$ is an arbitrary subset of joint domains that will be discussed in Section 2.3, and the joint design variables, $\kappa_e^{i,j}$, belong to the joint

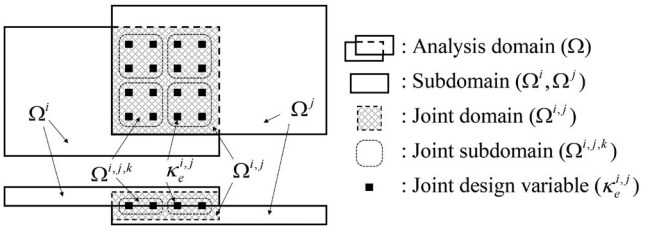

Figure 2. Definition of analysis domain, subdomain, joint domain, joint subdomain and joint design variable for general analysis domain.

domain $\Omega^{i,j}$. The joint subdomain, $\Omega^{i,j,k}$, also belongs to the joint domain $\Omega^{i,j}$. The compliance minimization problem can be formulated as follows:

$$\begin{aligned} &\underset{\mathbf{x}}{\text{Min}} \qquad c = \mathbf{F}^{\mathrm{T}}\mathbf{U} \\ &\text{subject to :} \\ &\qquad V^i(\boldsymbol{\gamma}) = \sum_{\text{Inside } \Omega^i} \gamma_e^i \le V_{\max}^i \\ &\qquad V^{i,j}(\boldsymbol{\kappa}) = \sum_{\text{Inside } \Omega^{i,j}} \kappa_e^{i,j} \le V_{\max}^{i,j} \\ &\qquad \varphi^{i,j} \le 0 \\ &\qquad T_{\max}^i \le T_0 \\ &\qquad \eta^{i,j} \le 0 \\ &\qquad \mathbf{KU} = \mathbf{F} \\ &\qquad \mathbf{x} = [\boldsymbol{\gamma}, \boldsymbol{\kappa}] \\ &\qquad (i, j = 1, 2, \ldots, m,\ i \ne j). \end{aligned} \tag{3}$$

The objective function, c, is set to the static compliance with respect to the design variable $\mathbf{x}$. The stiffness matrix, the displacement vector and the force vector are denoted by $\mathbf{K}$, $\mathbf{U}$ and $\mathbf{F}$, respectively. Because the design domain Ω is divided into several subdomains Ω^i and joint domains $\Omega^{i,j}$, the volume constraints are composed of two parts, one is the maximum volume constraint in each subdomain and the other is the constraint limiting the maximum number of joints in each joint domain. The maximum volume is set to $V_{\max}^i$ and the maximum number of joints is set to $V_{\max}^{i,j}$. The maximum number of joint constraints is not considered for the example problems except for Figure 7(a). The next constraint, $\varphi^{i,j}$, is the joint dispersal constraint, which is formulated to distribute the joints in the joint domain $\Omega^{i,j}$. The joint dispersal constraint is one of the contributions of the present study and will be discussed in the next subsection. The one-component constraint, $T_{\max}^i$, and the no-overlap constraint, $\eta^{i,j}$, control the shape of each subdomain and are considered only in three-dimensional problems. The one-component constraint and the no-overlap constraint will be discussed in Section 3.4. The design variable $\mathbf{x}$ is also divided into two sets of design variables. The first set consists of the topological design variables $\boldsymbol{\gamma}$ defining the topology of the structure in the subdomains, and the second set consists of the joint design variables $\boldsymbol{\kappa}$ defining the joints in the joint domains. The topological design variables $\boldsymbol{\gamma}$ in the subdomains are defined as follows:

$$\begin{aligned} \boldsymbol{\gamma} &= \left[\left[\gamma_1^1, \ldots, \gamma_{N^1}^1\right], \ldots, \left[\gamma_1^i, \ldots, \gamma_e^i, \ldots, \gamma_{N^i}^i\right], \ldots, \left[\gamma_1^m, \ldots, \gamma_{N^m}^m\right]\right] \\ &\quad i = 1, 2, \ldots, m, \quad \mathbf{0} \le \boldsymbol{\gamma}_{\min} \le \boldsymbol{\gamma} \le \mathbf{1}. \end{aligned} \tag{4}$$

The design variable γ_e^i denotes the e-th design variable in the i-th subdomain. The number of topological design variables for the i-th subdomain is N^i. The total number of subdomains is denoted by m and the minimum value of the design variables γ_e^i is set to 10^{-4}. Similar to topological density $\boldsymbol{\gamma}$, the normalized joint design variables $\boldsymbol{\kappa}$ in joint domains are defined as follows:

$$\boldsymbol{\kappa} = \left[\left[\kappa_1^{1,2},\ldots,\kappa_{N^{1,2}}^{1,2}\right],\ldots,\left[\kappa_1^{i,j},\ldots,\kappa_e^{i,j},\ldots,\kappa_{N^{i,j}}^{i,j}\right],\ldots,\left[\kappa_1^{m-1,m},\ldots,\kappa_{N^{m-1,m}}^{m-1,m}\right]\right]$$
$$i,j=1,2,\ldots,m,\quad i\neq j,\quad \mathbf{0}\leq\boldsymbol{\kappa}\leq\mathbf{1}. \tag{5}$$

The normalized joint design variable $\kappa_e^{i,j}$ denotes the e-th design variable in the joint domain $\Omega^{i,j}$. Unlike topological design variables, the minimum value of the joint design variables is set to zero, which can make completely unconnected regions be in a joint domain.

In the above optimization formulation (3)–(5), the k-th joint subdomain is defined as follows:

$$\Omega^{i,j,k}\subset\Omega^{i,j},\quad \Omega^{i,j,1}\cup\Omega^{i,j,2}\cup\cdots\cup\Omega^{i,j,m^{i,j}}=\Omega^{i,j}, \tag{6}$$

where the number of joint subdomains is denoted by $m^{i,j}$; further details will be discussed in Section 2.3. The formulation of the joint modelling and the joint dispersal constraint will be discussed in the next section.

2.2. Joint modelling for multiple subdomains

This subsection develops a new formulation regarding the joint stiffness, $\mathbf{K}_{\text{joint}}$. The terms '*connecting*' and '*joining*' mean that, from an engineering point of view, the displacements of the connected nodes should be set to be the same. In order to address the issue of the joint, this research considers the two joint models in Figure 3. The concepts of 'NSJ' and 'ESJ' are proposed in the present research. The first joint model, called the Node Spring Joint (NSJ) model here in Figure 3(a:left-bottom), is a method of connecting nodes at the same locations with zero-length rigid springs. The other joint model, called the Element Spring Joint (ESJ) model in Figure 3(a:right-bottom), is a method of connecting the nodes of elements at the same location with multiple zero-length rigid springs. For example, the four springs defined at one-quad elements have the same springs joining the displacements of the nodes in the ESJ model. The stiffness of the joint depends on the design variables as follows:

$$\mathbf{K}_{\text{joint}}(\boldsymbol{\gamma},\boldsymbol{\kappa})=\sum_{i=1}^{m}\sum_{j=1,i\neq j}^{m}\sum_{e=1}^{N^{i,j}}\mathbf{K}_e^{i,j}, \tag{7}$$

where $\mathbf{K}_e^{i,j}$ is the joint stiffness matrix connecting the i-th and j-th subdomains.

The NSJ modelling is straightforward to implement, but from an optimization point of view, a singular problem causing a rigid body mode can occur as shown in Figure 3(c:top). On the other hand, as one ESJ joint connects multiple nodes, it can remove a rigid body mode as shown in Figure 3(c:bottom). In this study, the ESJ method is employed for joint modelling and the stiffness values are interpolated as follows:

$$\mathbf{K}_e^{i,j}=f(\kappa_e^{i,j})\gamma_{\text{Adjacent}}^{i}\gamma_{\text{Adjacent}}^{j}\mathbf{K}_{\text{nominal}}^{i,j} \tag{8}$$

$$f(\kappa_e^{i,j})=\frac{(\kappa_e^{i,j})^n}{1+(1-(\kappa_e^{i,j})^n)\frac{l_{\max}^{i,j}}{k_{\text{diagonal}}^{\text{structure}}\times\dim}}. \tag{9}$$

The above interpolation function in (9) can be beneficial to the convergence of the joint design variables. Assigning a larger value for the maximum stiffness value causes a convergence issue in

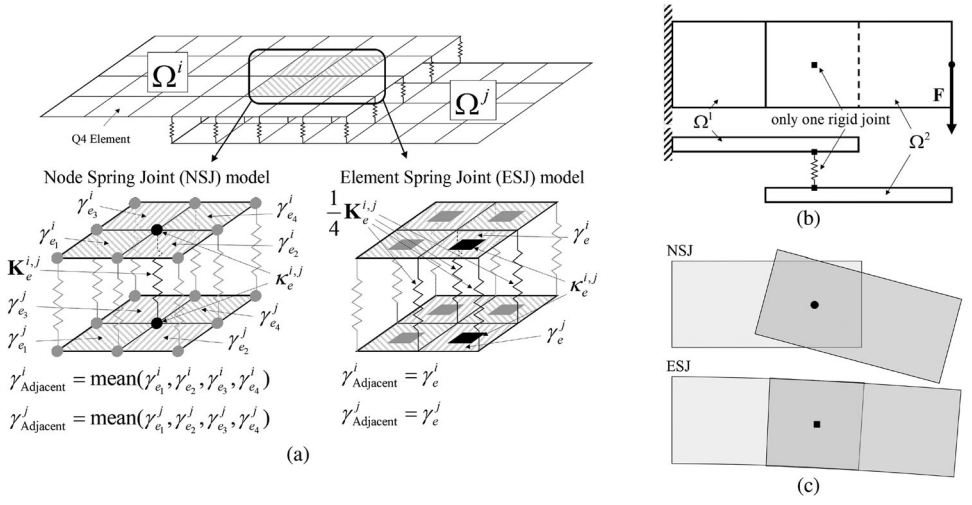

Figure 3. Schematics for the two joint modelling types in the joint domain: (a) the NSJ model approach connecting the individual nodes with the same locations, the ESJ model approach connecting the individual elements with the same locations; (b) only-one-rigid-spring model; and (c) rigid body motion for each joint model.

a topology optimization process when the SIMP method is implemented to calculate joint stiffness. Therefore, this research proposes utilizing the above interpolation in Yoon *et al.* (2008). The convergence of the joint design variables is improved with the above interpolation function.

The nominal stiffness of the spring is denoted by $\mathbf{K}^{i,j}_{\text{nominal}}$, defined as follows:

$$\mathbf{K}^{i,j}_{\text{nominal}} = \begin{array}{c} \begin{matrix} u_{1x} & u_{1y} & u_{2x} & u_{2y} \end{matrix} \\ \begin{pmatrix} l^{i,j}_{\max} & 0 & -l^{i,j}_{\max} & 0 \\ 0 & l^{i,j}_{\max} & 0 & -l^{i,j}_{\max} \\ -l^{i,j}_{\max} & 0 & l^{i,j}_{\max} & 0 \\ 0 & -l^{i,j}_{\max} & 0 & l^{i,j}_{\max} \end{pmatrix} \end{array} \tag{10}$$

$$l^{i,j}_{\max} = \alpha^{i,j}_{\max} \times \text{mean}(\text{diag}(\mathbf{K}^{i}_{\text{nominal}}), \text{diag}(\mathbf{K}^{j}_{\text{nominal}})), \tag{11}$$

where the maximum stiffness of a joint is denoted by $l^{i,j}_{\max}$. The maximum stiffness $l^{i,j}_{\max}$ is proportional to the average value of the diagonal components of connected nominal stiffness. In the present study, a value of 10^3 is chosen for $\alpha^{i,j}_{\max}$ to prevent numerical error and to keep the displacement error sufficiently small compared with ideal rigid springs. Detailed information is described in the online supplemental data for this article, which can be accessed from https://doi.org/10.1080/0305215X.2022.2089879.

2.3. Joint dispersal constraint and joint subdomains

As joints are defined at finite element nodes, the mesh dependency of optimized joints is inevitably observed. With a refined quad element, the total number of possible joints may increase, and also the gap between joints may decrease, which may cause the clustering of joints. The positions of joints depend on an objective function and a number of joint constraints in the joint subdomain. Therefore, an alternative approach evenly distributing joints may help a local optimizer to relieve the mesh dependency. Indeed, this subsection develops a Joint Dispersal (JD) constraint to overcome the mesh-dependency problem and keep a minimum distance between joints.

Table 1. JD constraint values using various different joint design variables.

$\kappa_e^{i,j}$ variables	$\sum_{\text{Inside }\Omega^{i,j,k}} \kappa_e^{i,j}$	$\max_{\text{Inside }\Omega^{i,j,k}} \kappa_e^{i,j}$	$\varphi^{i,j,k}$ constraint value
{0, 1, 0, 0}	1	1	0 (active)
{0, 1, 1, 0}	2	1	1 (violated)
{0, 0, 0, 0}	0	0	0 (active)

Before explaining the JD constraint, the *joint domain* $\Omega^{i,j}$ and the *joint subdomain* $\Omega^{i,j,k}$ should be defined. The joint domain between the subdomains Ω^i and Ω^j is defined as $\Omega^{i,j}$. Each joint domain is further divided into several arbitrarily-shaped joint subdomains $\Omega^{i,j,k}$ $(k = 1, 2, \ldots, m^{i,j})$, which can overlap the other joint subdomains. Joints in $\Omega^{(i,j)}$ can be defined in several other joint subdomains for the JD constraint $\varphi^{(i,j,k)}$ because the joint subdomains can overlap the other joint subdomains. These characteristics of joint subdomains play an important role in controlling the distance between joints.

$$\varphi^{i,j,k} = \sum_{\text{Inside }\Omega^{i,j,k}} \kappa_e^{i,j} - \max_{\text{Inside }\Omega^{i,j,k}} (\kappa_e^{i,j}) \approx \sum_{\text{Inside }\Omega^{i,j,k}} \kappa_e^{i,j} - \left[\sum_{\text{Inside }\Omega^{i,j,k}} (\kappa_e^{i,j})^{p_1} \right]^{1/p_1} \leq 0. \tag{12}$$

The above equation (12) states that the *sum* of the joint design variables must be less than or equal to the *maximum* joint design variables inside the joint subdomain $\Omega^{i,j,k}$. With this condition, a maximum of one joint design variable is allowed for each joint subdomain in Table 1. To incorporate the constraint into the gradient-based optimizer, a p-norm value with $p_1 = 20$ is employed where the JD constraint error is small enough (refer to the online supplemental data). The differentiation of the above constraint with respect to the design variables can be obtained easily.

$$\varphi^{i,j} = \left(\left[\sum_{k=1}^{m^{i,j}} \left(\varphi^{i,j,k} \right)^{p_2} \right]^{1/p_2} \Big/ \, m^{i,j} \right) - \varepsilon_1 \leq 0, \quad \varepsilon_1 = 10^{-5}. \tag{13}$$

The above constraint (13) is defined at every joint subdomain and further aggregated to reduce the number of constraints to $\varphi^{i,j}$. The joint subdomains are defined to be of circular shape with diameter $\delta_{\min}$ at every joint in Figure 4(a). When the JD constraint (13) is ideally satisfied, the distances between all joints must be greater than $\delta_{\min}$. But, in Figure 4(b), when the $\delta_{\min}$ value is equal to a multiple of the mesh size, the minimum distance between joints must be greater than the intended $\delta_{\min}$ value. And to solve this side effect, the distance between joints should be less than the $\delta_{\min}$ value when the $\delta_{\min}$ value is set to a value smaller than that in Figure 4(c). To resolve this side effect with circular joint subdomain, some cares should be made. Due to the mesh dependency, all of the joint subdomain is further divided into four domains as shown in Figure 5. In other words, the circular joint subdomains for the JD constraint in Figure 5(a) is decomposed into the four modified circular shapes illustrated in Figure 5(b) and the calculations of the joint subdomains are carried out for each joint subdomain. A sensitivity analysis of the joint dispersal constraint is described in the online supplemental data.

3. Numerical examples

To show the topology optimization application considering joints connecting multiple components with the JD constraint, this section presents several topology optimization results. The compliance minimization problem is considered with the volume constraint and the joint dispersal constraint. The Method of Moving Asymptotes (MMA) algorithm (Svanberg 1987) is employed in the optimization algorithm.

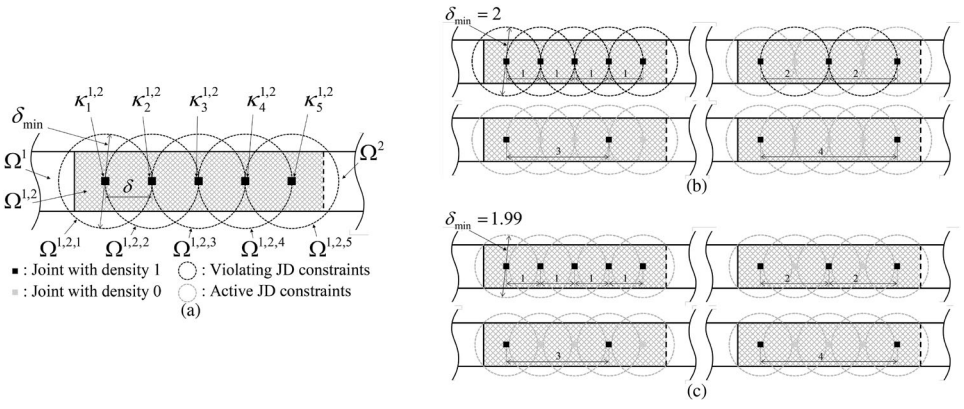

Figure 4. Definition of joint subdomains and its side effects: (a) assume that five joints are arranged in a line at equal intervals, $\delta = 1$ and also that five joint subdomains, which are dotted circles of diameter $\delta_{min} = 2$, are assigned to each joint; (b) the satisfaction of JD constraints is shown for various joint locations; (c) the side effect when the diameters of joint subdomains are 1.99.

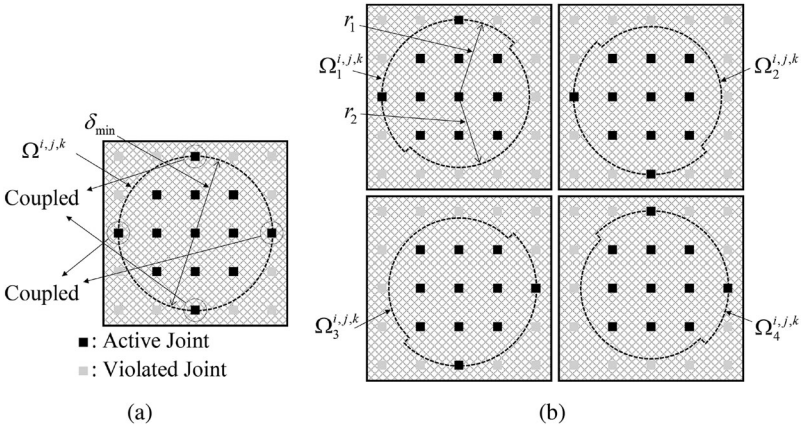

Figure 5. A modification of the subdomain to overcome the effect of the boundary of the subdomain: (a) a conventional circular joint subdomain causing an unprecise joint distance constraint; and (b) a presented shape with four overlapping subdomains to represent the joint distance of a combination of semicircles.

3.1. Example 1: Cantilever design problem with two subdomains

To illustrate the effect of the JD constraint on a multiple-component optimization problem, a two-dimensional cantilever problem with two subdomains (Ω^1 and Ω^2) is considered in Figure 6(a). The size of the optimization problem is assumed to be 24 by 8 m with thickness 1 m and it is assumed that the two subdomains (16 by 8 m) overlap in the central domain $\Omega^{1,2}$ (8 by 8 m). Each subdomain is discretized by 64 by 32 four-node quad elements. The left-hand side of the first subdomain is clamped and a point load of 1000 N is applied in the $-y$-direction at the right-hand side of the second subdomain. With the topology optimization formulation and a single subdomain, the optimized design in Figure 6(b) can be obtained with 1.1197 mJ as the objective function with 40% of the volume constraint. For the topology optimization with two components, the total volume of the two subdomains in Figure 7 is set to be the same, *i.e.* 40% = 2 × (2/3) × (the volume ratio of each subdomain, *i.e.* 30%).

The optimized layouts without and with the joint dispersal constraint using the ESJ method are shown in Figures 7(a) and 7(b), respectively. In Figures 7(a) and 7(b), the first illustration shows the topological layout of the joints. The second and fourth illustrations show the topological layouts of

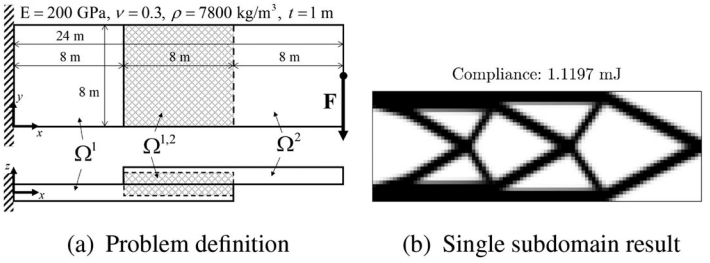

Figure 6. Example 1: Cantilever beam problem: (a) problem definition (two subdomains: Ω^1 and Ω^2, one overlapping joint domain, $\Omega^{1,2}$); and (b) a topology optimization result with a single model and a 40% volume ratio (1.1197 mJ).

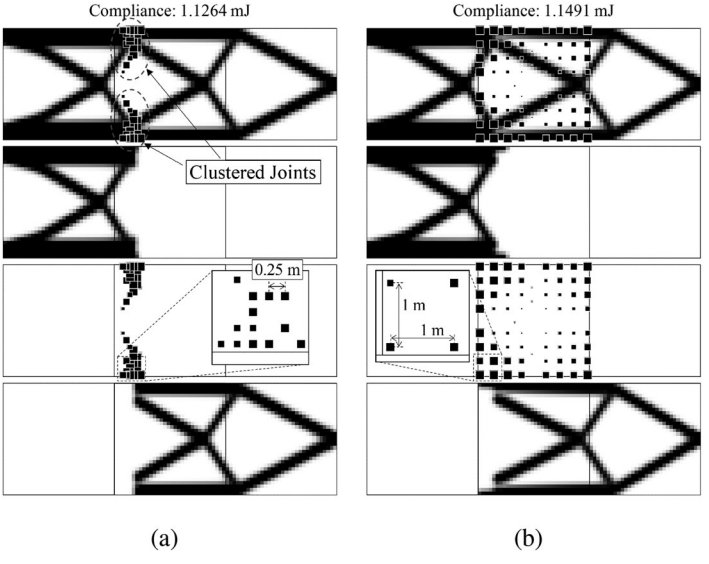

Figure 7. Optimization results with joint interpolation function $\mathbf{K}_e^{i,j} = (\kappa_e^{i,j})^n \mathbf{K}_{\text{nominal}}^{i,j}$: (a) optimized layout *without* the joint dispersal constraint (1.1264 mJ); (b) optimized layout *with* the joint dispersal constraint (1.1491 mJ).

each subdomain, and the third illustration shows the distribution of the joints. The black rectangular boxes represent the joints connecting the two subdomains. The volume ratio of each subdomain is set to 30%. The number of joint constraints, $V_{\max}^{1,2}$ in (3), is set to 51 (5%) only in Figure 7(a) and is not assigned for the joint domain in Figure 7(b). The SIMP interpolation function for joint stiffness ($\mathbf{K}_e^{i,j} = (\kappa_e^{i,j})^n \mathbf{K}_{\text{nominal}}^{i,j}$) is used only in Figure 7 to find the effect of the JD constraint. The polynomial interpolation function (8) is used in all the remaining examples. By investigating the optimized layout in Figure 7(a) without the joint dispersal constraint, it is observed that the joints are very clustered with some unnecessary joints in the empty space of the joint domain. The distance between joints is 0.25 m, which is the same as the mesh size. With the joint dispersal constraint ($\delta_{\min} = 1$ m), the minimum distance between joints can be controlled for the optimized layouts in Figure 7(b) and, according to the JD constraint, the distance between joints is increased by 1 m. But when the distance between joints satisfies the JD constraint in Figure 7(b), there is a problem that some joints appears in the empty region. To remove the joints from the empty region, the joint stiffness interpolation function (8) is used in all remaining examples.

To find the effect of the minimum joint distance constraint value, the parameter $\delta_{\min}$ is adjusted by 1, 2, 3 and 4 m in Figure 8. When the minimum joint distance parameters are getting increased, the number of joints is decreased without limiting the maximum number of joints. In other words, the optimization algorithm can decide the number of necessary joints and distribute them in the design

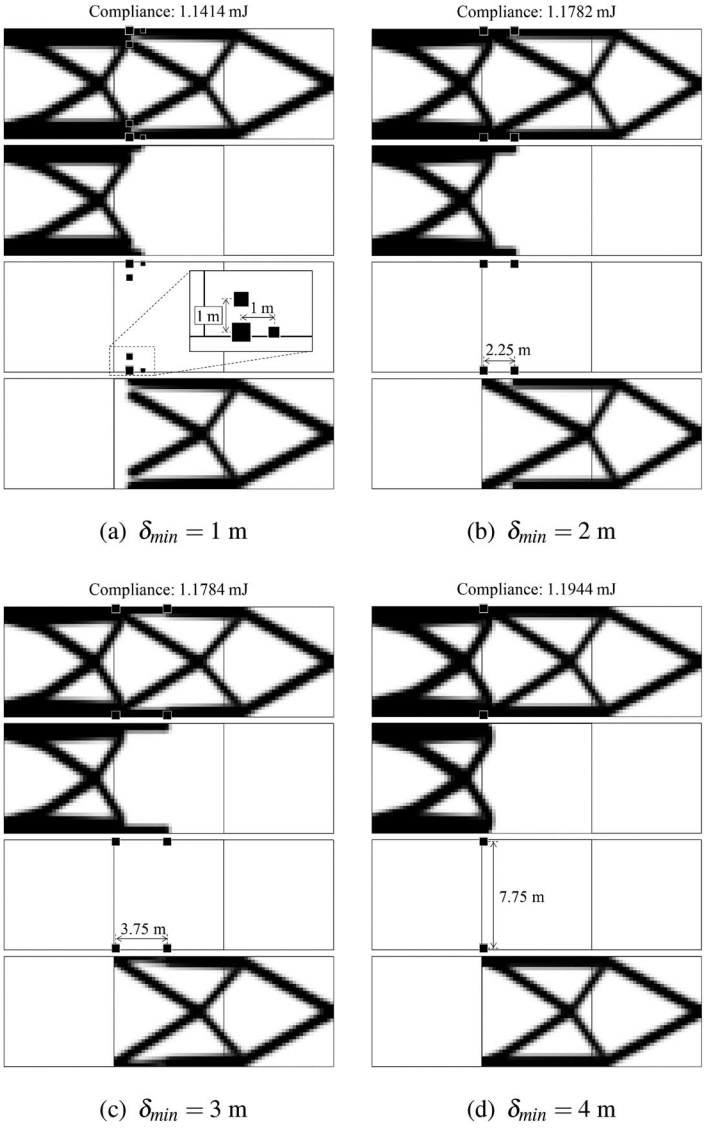

Figure 8. Topology optimization results for cantilever problem with different minimum joint distance parameters ($\delta_{\min}$). (a) $\delta_{\min} = 1$ m. (b) $\delta_{\min} = 2$ m. (c) $\delta_{\min} = 3$ m and (d) $\delta_{\min} = 4$ m.

space while satisfying the minimum joint distance constraints. It is observed that, with the different values for $\delta_{\min}$, the topological layouts of each subdomain with some differences near the optimized joints are obtained. The joints on the left-hand side of the joint domain appear at the right-hand side by increasing the $\delta_{\min}$ value with a slightly increased compliance. This is because the design space is further limited from an optimization point of view by adding the joint dispersion constraint.

The topological layout for different mesh sizes is shown in Figure 9. The optimization parameters are the same as the parameters in Figure 8(a) with different numbers of degrees of freedom. As the number of degrees of freedom increases, the locations of joints are changed while maintaining the distances between joints. Using the joint dispersal constraint, a minimum distance between all joints can be maintained regardless of the mesh size.

In the present study, the mass constraints are defined for each subdomain. Because the mass constraints affect the optimized layouts for each subdomain, the optimized joints are also influenced. For

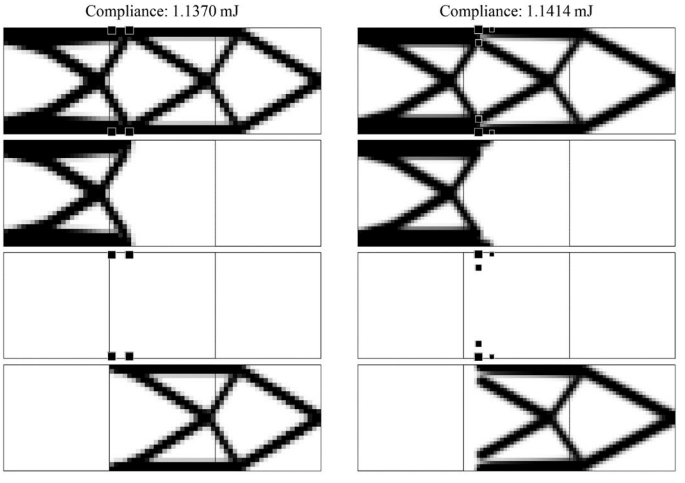

(a) Number of degrees of freedom: 4900 (b) Number of degrees of freedom: 8580

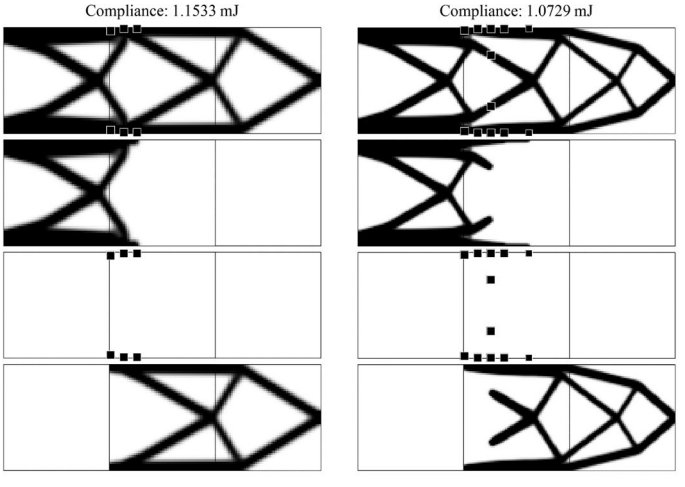

(c) Number of degrees of freedom: 19012 (d) Number of degrees of freedom: 33540

Figure 9. Topology optimization results for different mesh refinements with $\delta_{\text{min}} = 1$ m. The optimization parameters are the same except for the mesh size. The total numbers of degrees of freedom are: (a) 4900; (b) 8580; (c) 19,012; and (d) 33,540.

example, Figure 10(a) shows optimization layouts with different mass ratios for the first subdomain and the second subdomain; with 20% for the first subdomain, the optimized layout appears on the left-hand side only. Indeed, the joints appear on the left-hand side of the optimized layout for the first subdomain connecting with the optimized layout in the second subdomain. This phenomenon is reversed by changing the mass ratios as shown in Figure 10(b). It is possible to impose a total mass constraint, *i.e.* the summation of the masses of all subdomains. However, this increases the design space from an optimization point of view.

As the presented algorithm uses a gradient based optimizer, some grey elements inevitably appear for joints as well as layouts. Therefore, a postprocessing for layouts and joints is required. For example, Figure 11(a) shows the joint distributions, *i.e.* $f(\kappa_e^{1,2})\gamma^1_{\text{Adjacent}}\gamma^2_{\text{Adjacent}}$, as well as the layout. Figure 11(b) shows the distributions of f values. It can be observed that the intermediate joints appear at the

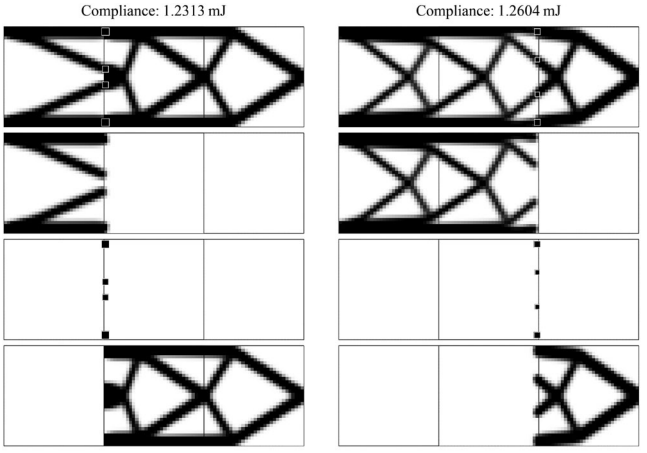

(a) Volume fraction: 20%, 40% (b) Volume fraction: 40%, 20%

Figure 10. The effect of the mass constraint: (a) volume fraction: 20% for the first subdomain and 40% for the second subdomain; and (b) volume fraction: 40% for the first subdomain and 20% for the second subdomain.

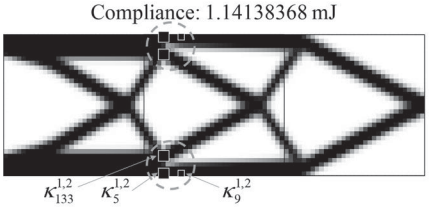

	$\kappa_5^{1,2}$	$\kappa_9^{1,2}$	$\kappa_{133}^{1,2}$
$\kappa_e^{1,2}$	0.999962	0.999967	0.999980
$f(\kappa_e^{1,2})$	0.946453	0.952452	0.970164
$\gamma_{\text{Adjacent}}^1$	0.999718	0.418638	0.999586
$\gamma_{\text{Adjacent}}^2$	0.971228	0.999830	0.750638
$f(\kappa_e^{1,2})\gamma_{\text{Adjacent}}^1\gamma_{\text{Adjacent}}^2$	0.918962	0.398664	0.727940

(a)

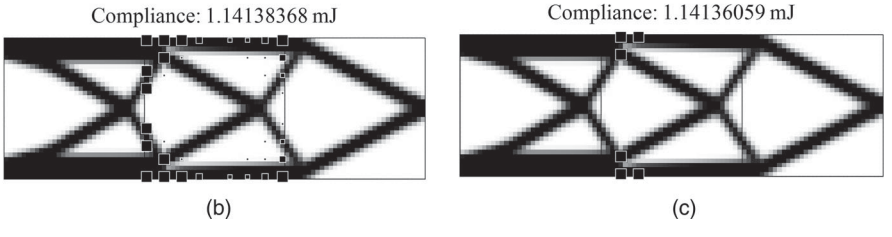

(b) (c)

Figure 11. Joint distributions and joint values: (a) optimized layout of Example 1 (joint plot with $f(\kappa_e^{1,2})\gamma_{\text{Adjacent}}^1\gamma_{\text{Adjacent}}^2$) and the design variables; (b) distributions of the design variables with $f(\kappa_e^{1,2})$; and (c) postprocessed compliance (for comparison, six decimal places and eight decimal places are employed for the design variable and compliance, respectively).

upper and bottom corners marked by circles in Figure 11(a). The intermediate design variables for $\gamma_{\text{Adjacent}}^1$ and $\gamma_{\text{Adjacent}}^2$ are 0.418,638 and 0.999,830 for joint $\kappa_9^{1,2}$; for comparison, six digits after the decimal point are employed. To investigate the effect of these intermediate joints, the postprocessing setting $\gamma_{\text{Adjacent}}^1$ and $\gamma_{\text{Adjacent}}^2$ of the intermediate joints is carried out in Figure 11(c). As shown, the compliance is slightly decreased. In addition, note that the maximum joint stiffness value is chosen very high; in this example, 10^3 times larger than the nominal stiffness value of the plane element. From an engineering point of view, the effect of the intermediate joint therefore can be neglected after postprocessing. To remove these joints with intermediate stiffness values, some other techniques can be employed.

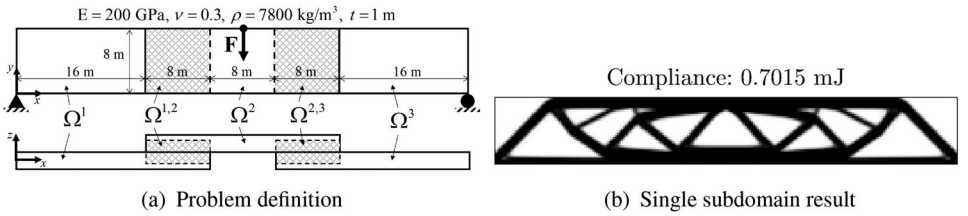

(a) Problem definition (b) Single subdomain result

Figure 12. Example 2: The MBB problem: (a) problem definition with three subdomains (Ω^1, Ω^2 and Ω^3), and two overlapping joint domains ($\Omega^{1,2}$ and $\Omega^{2,3}$); and (b) a topology optimization result for the single model with 51.43% volume ratio (0.7015 mJ).

3.2. Example 2: MBB problem with three subdomains

For the second example, the Messerschmitt–Bolkow–Blohm (MBB) beam problem with three subdomains (Ω^1, Ω^2 and Ω^3) and two joint domains ($\Omega^{1,2}$ and $\Omega^{2,3}$) is considered in Figure 12. A 1000 N force is applied in the $-y$-direction at the centre of the upper domain. The bottom-left corner of the first subdomain is fixed, and the bottom-right corner of the third subdomain is fixed only in the y-direction. The optimized layout with a single domain is presented in Figure 12(b) with 0.7015 mJ for its compliance. The volume ratio for the single subdomain is set to 51.43%, which is the same as the summation for the three subdomains, *i.e.* 51.43% $= 3 \times 3/7 \times$ (the volume ratio of each subdomain, *i.e.* 40%).

Figure 13 shows the optimized layouts with the different joint distance values $\delta_{\min}$. The volume ratio of each subdomain is set to 40%. The optimized layouts satisfying the joint distance constraints can be successfully obtained. The first illustration in each part figure shows the overall structure with optimized joints. The second, fourth and sixth illustrations show the optimized topological layouts, and the third and the fifth illustrations show the optimized joints. With larger distances between the joints, some joints are dispersed, and the object value is increased accordingly as in the first example. Unlike the case of the first example, the overall topological results of each subdomain change slightly with increasing $\delta_{\min}$ value for the different positions of the joints. By investigating the optimized layouts, it is observed that, with larger distances between the joints, the number of joints also decreases.

3.3. Example 3: Kirchhoff's shell problem with two subdomains

The present optimization framework can be applied for the shell structure. To show the application, Figures 14 and 15 show the optimization results for domains modelled by Kirchhoff shell elements. The design domains are discretized with 64 by 32 four-node shell elements. The minimum joint distance value $\delta_{\min}$ and the maximum volume ratio $V^i_{\max}$ are set to 2 m and 30%, respectively. With the joint distance constraint, the two plates are designed with optimized joints. In order to model the joints for shell elements having rotational degrees of freedom, it is necessary to modify the link stiffness matrix (10) as follows:

$$\mathbf{K}^{i,j}_{\text{nominal}} = \begin{array}{c} \begin{matrix} w_1 & \theta_{x1} & \theta_{y1} & w_2 & \theta_{x2} & \theta_{y2} \end{matrix} \\ \begin{pmatrix} l^{i,j}_{\text{tr}} & 0 & 0 & -l^{i,j}_{\text{tr}} & 0 & 0 \\ 0 & l^{i,j}_{\text{rot}} & 0 & 0 & -l^{i,j}_{\text{rot}} & 0 \\ 0 & 0 & l^{i,j}_{\text{rot}} & 0 & 0 & -l^{i,j}_{\text{rot}} \\ -l^{i,j}_{\text{tr}} & 0 & 0 & l^{i,j}_{\text{tr}} & 0 & 0 \\ 0 & -l^{i,j}_{\text{rot}} & 0 & 0 & l^{i,j}_{\text{rot}} & 0 \\ 0 & 0 & -l^{i,j}_{\text{rot}} & 0 & 0 & l^{i,j}_{\text{rot}} \end{pmatrix} \end{array} \tag{14}$$

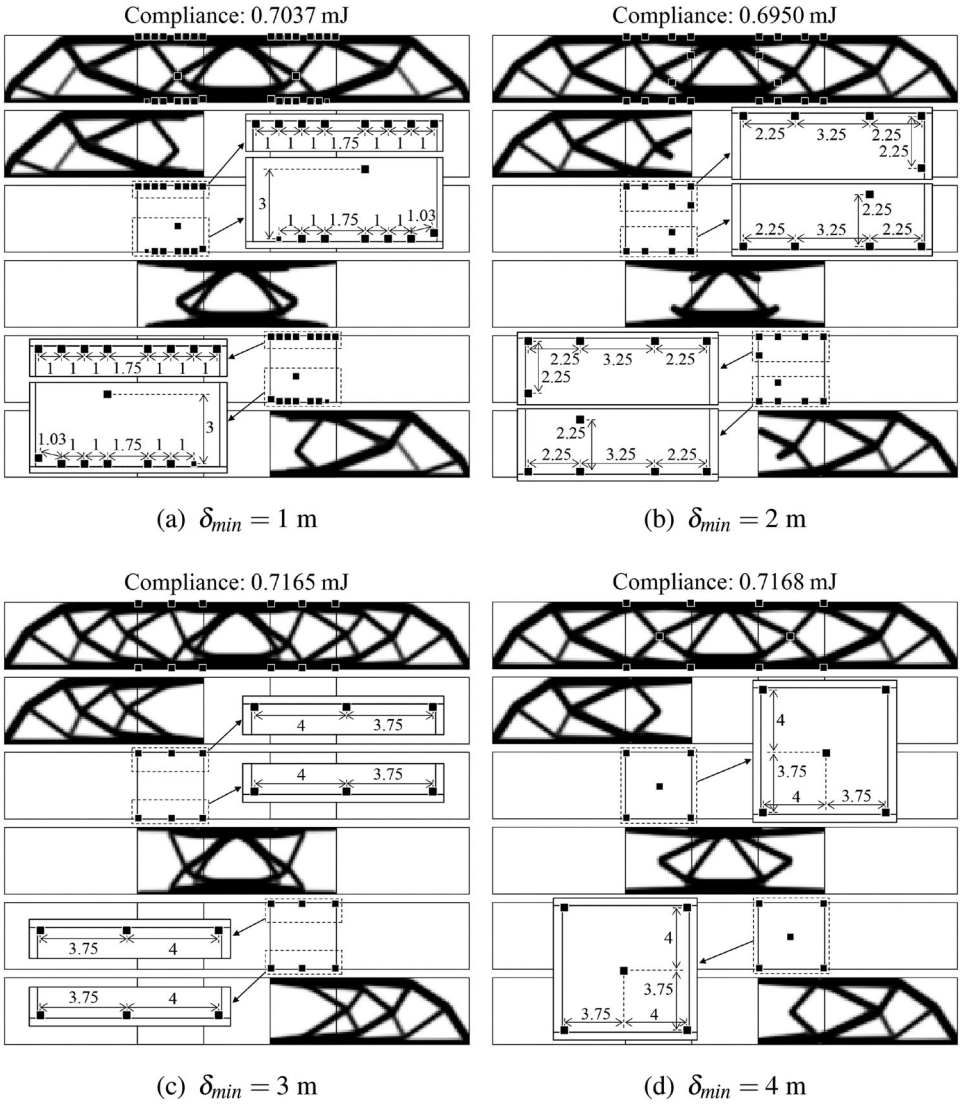

Figure 13. Topology optimization results for the MBB problem with different minimum joint distance parameters ($\delta_{\min}$). All distance values between joints are in metres. (a) $\delta_{\min} = 1$ m. (b) $\delta_{\min} = 2$ m. (c) $\delta_{\min} = 3$ m and (d) $\delta_{\min} = 4$ m.

$$
\begin{aligned}
l_{\text{tr}}^{i,j} &= \alpha_{\max}^{i,j} \times \text{mean}(\text{diag}(\mathbf{K}_{\text{tr}}^{i}), \text{diag}(\mathbf{K}_{\text{tr}}^{j})) \\
l_{\text{rot}}^{i,j} &= \alpha_{\max}^{i,j} \times \text{mean}(\text{diag}(\mathbf{K}_{\text{rot}}^{i}), \text{diag}(\mathbf{K}_{\text{rot}}^{j})),
\end{aligned}
\tag{15}
$$

where the maximum connection stiffness is separated by translation part ($l_{\text{tr}}^{i,j}$) and rotation part ($l_{\text{rot}}^{i,j}$). The translation stiffness is calculated by the average of the diagonal components of connected nominal translation stiffness, and the rotation stiffness is calculate using the connected nominal rotation stiffness. The $\alpha_{\max}^{i,j}$ value is set to 10^3, which is the same as for previous examples.

For the bending load in Figure 14(a), the U-shape with a sharp end and two supporting structures is obtained for the single-subdomain result in Figure 14(b). In Figure 14(c), a sharp pin shape structure appears in the second subdomain and three structures appear for the first domain to support the load carried from the second subdomain. For the torsional load in Figure 15(a), the thick cantilever shape

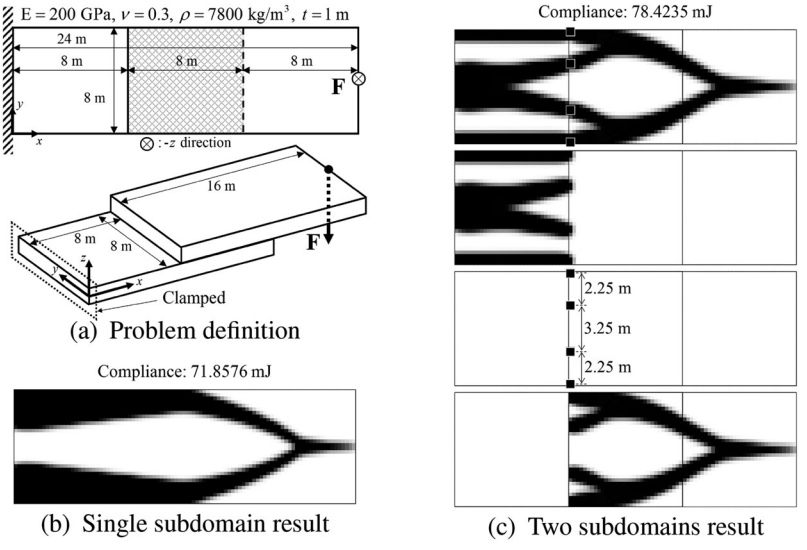

Figure 14. Example 3.1: Shell plate with a point load: (a) problem definition with two subdomains; (b) optimized result for a single-subdomain model with a 40% volume ratio (71.8576 mJ); and (c) for a two-subdomain model (78.4235 mJ).

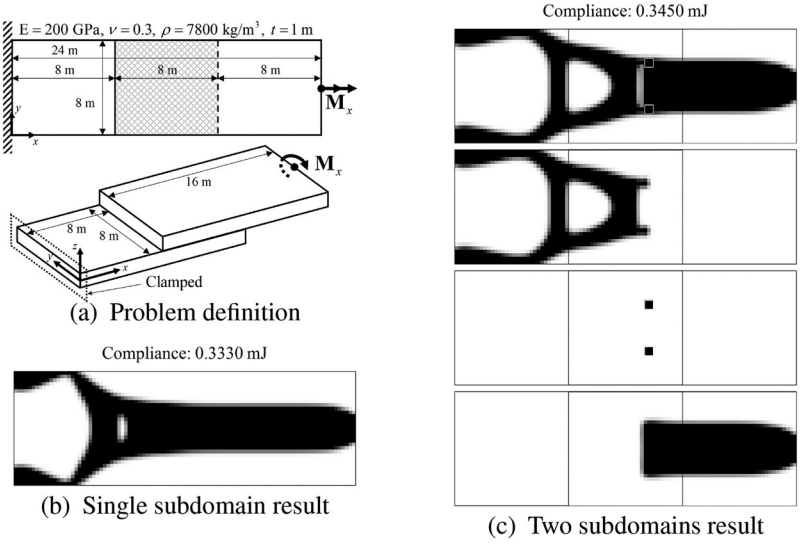

Figure 15. Example 3.2: Shell plate with a bending load: (a) problem definition with two subdomains; (b) optimized result for a single-subdomain model with a 40% volume ratio (0.3330 mJ); and (c) for a two-subdomain model (0.3450 mJ).

with two supporting structures is optimized for the single-subdomain result in Figure 15(b). In the case of the two-subdomain result in Figure 15(c), a thick bar-shaped structure appears in the second subdomain. To resist the bending load effectively, a structure connected to the structure in the first subdomain at the four different locations can be obtained. In the middle of the structure, vertical bars can be obtained to increase the torsional stiffness.

3.4. Example 4: 3D cantilever problem with two subdomains

As a final example, the 3D cantilever problem with two subdomains is considered in Figure 16 . In the middle of the two subdomains, one joint subdomain is defined. The size of the optimization problem

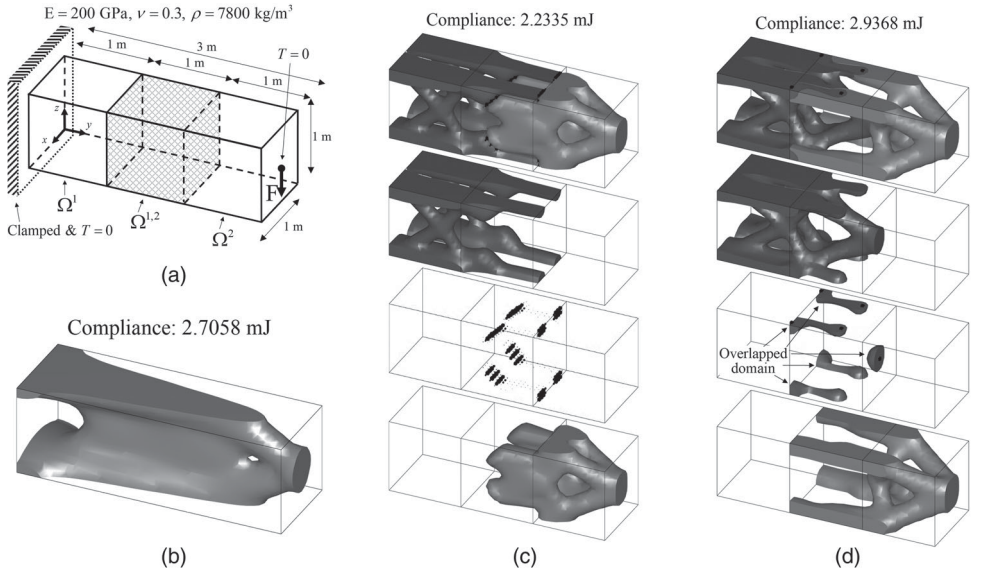

Figure 16. Example 4: 3D cantilever problem with a point load: (a) problem definition with two subdomains; (b) single-subdomain result with a 26.67% volume ratio; (c) results with a 20% volume ratio for each subdomain without a JD constraint; and (d) without a no-overlap constraint but with a JD constraint ($\delta_{\min} = 0.5$ m).

is 1 by 3 by 1 m and it is assumed that two subdomains 1 by 2 by 1 m overlap in the central domain $\Omega^{1,2}$. Each of the subdomains is discretized by 16 by 32 by 16 eight-node cube elements. The left-hand side of the first subdomain is clamped and a point load of 1000 N is applied in the $-z$-direction at the right-hand side of the second subdomain. The volume ratio of each subdomain is set to 20%. The nominal stiffness of the three-dimensional spring in (10) is redefined as follows:

$$\mathbf{K}^{i,j}_{\text{nominal}} = \begin{array}{c} \begin{matrix} u_{1x} & u_{1y} & u_{1z} & u_{2x} & u_{2y} & u_{2z} \end{matrix} \\ \begin{pmatrix} l^{i,j}_{\max} & 0 & 0 & -l^{i,j}_{\max} & 0 & 0 \\ 0 & l^{i,j}_{\max} & 0 & 0 & -l^{i,j}_{\max} & 0 \\ 0 & 0 & l^{i,j}_{\max} & 0 & 0 & -l^{i,j}_{\max} \\ -l^{i,j}_{\max} & 0 & 0 & l^{i,j}_{\max} & 0 & 0 \\ 0 & -l^{i,j}_{\max} & 0 & 0 & l^{i,j}_{\max} & 0 \\ 0 & 0 & -l^{i,j}_{\max} & 0 & 0 & l^{i,j}_{\max} \end{pmatrix} \end{array}, \tag{16}$$

where the link stiffness is the same as in Equation (11) and the $\alpha^{i,j}_{\max}$ variable is also set to 10^3.

Unlike in two-dimensional problems with links whose directions are aligned in the out-of-plane direction, a one-component constraint and a no-overlap constraint are additionally considered in three-dimensional problems. The one-component constraint means that the number of components is controlled to be one. In three-dimensional problems, several components can appear. To overcome this aspect, the virtual temperature approach developed is implemented. In Quhao Li *et al.* (2016), the virtual temperature, T, is calculated and bounded to eliminate enclosed cavities in topology optimization. To modify the virtual temperature approach to the one-component constraint, the following modified heat conductivity, K_T, and the heat source condition, Q, are considered.

$$\begin{aligned} K_T(\gamma_e) &= \left(\gamma_{\min} + (\gamma_{\max} - \gamma_{\min})\,\gamma_e^{10}\right) K_{T_0} \\ Q(\gamma_e) &= \gamma_e Q_0. \end{aligned} \tag{17}$$

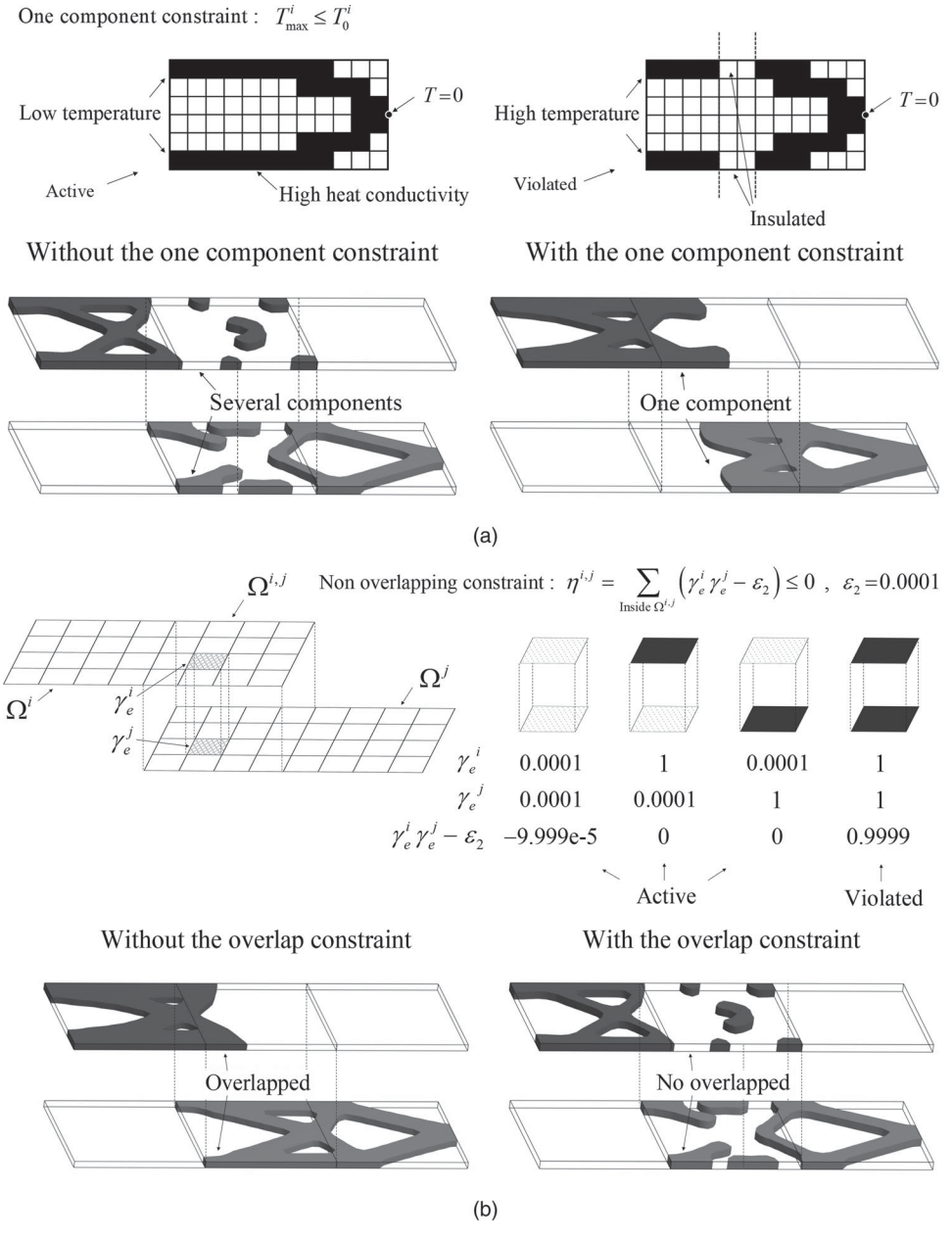

Figure 17. Schematics for two additional constraints in 3D cases: (a) a one-component constraint; and (b) a no-overlap constraint.

With this condition, the virtual temperature can be calculated and bounded to maintain one component. As an example, the optimum layout in Figure 17(a:left) with six distributed structures for the first component (relatively dark grey colour) and five distributed structures for the second component (relatively light grey colour) can be obtained. On the other hand, with the above equation (17), it is possible to maintain one-component structures in Figure 17(a:right).

$$T_{\max} \le T_0, \tag{18}$$

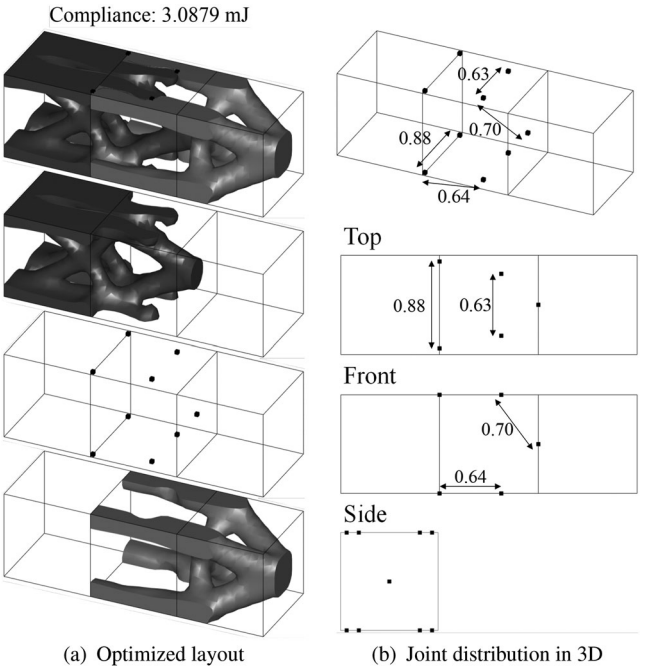

Figure 18. Example 4: (a) optimized result with 20% volume ratio for each subdomain; and (b) optimized joint distribution with 0.5 m minimum joint distance ($\delta_{\min} = 0.5$ m), and with no-overlap constraint. All distance values between joints are also in metres.

where the virtual temperature and the upper bound of the virtual temperature are set as $T_{\max}$ and T_0, respectively. The maximum temperature is obtained by the p-norm approach as follows:

$$T^i_{\max} \approx \left[\sum_{\text{Inside } \Omega^{i,j}} \left(T^i_e\right)^{p_3} \right]^{1/p_3}. \tag{19}$$

In the present study, the maximum temperature $T_{\max}$ is obtained with the p-norm formulation with $p_3 = 10$ for the penalization. The upper bound of the temperature T_0 is set to the temperature of the solid domain. To dissipate the heat in Figure 16(a), temperature boundary conditions are applied at the left-hand side of the first subdomain, and the point where the mechanical load is applied in the second subdomain. In addition to this, a no-overlap constraint among components is imposed as follows:

$$\eta^{i,j} = \sum_{\text{Inside } \Omega^{i,j}} (\gamma^i_e \gamma^j_e - \varepsilon_2) \le 0, \quad \varepsilon_2 = 10^{-4}. \tag{20}$$

With the above no-overlap constraint, $\eta^{i,j}$, the overlapping domain can be removed as shown in Figure 17(b:right).

Figure 18(a) shows the optimized layout for the three-dimensional problem in Figure 16(a). The nine joints can be distributed between the two components with $\delta_{\min} = 0.5$ m for the joint distance constraint as illustrated in Figure 18(b). Without the joint dispersal constraint, the aggregation of the joints appears as shown in Figure 16(c). Without the no-overlap constraint, the two components overlap as shown in Figure 16(d) with the overlap domain. Note that the optimized layout without the no-overlap constraint is stiffer than the optimized layout with the no-overlap constraint. A 3.0879 mJ compliance is obtained for the design in Figure 16(b), which is a 4.9% higher compliance than the 2.9368 mJ compliance of the design in Figure 18(a).

4. Conclusions

This study describes the development of topology optimization formulations for multi-component joint connectivity. When solving a multi-component problem, the positions of joints have great influence on the overall shape, stability and manufacturing condition of the structure. The design variables determining the joints as well as the design variables for optimizing the topology are optimized. From a finite element point of view, joints can be modelled using the rigid spring model. The optimization formulation minimizing compliance subject to the mass constraint finds optimized joints as well as optimized layouts simultaneously. Although the stiffness values of parts having topological design variables of low density value are small, the joint design variables appear at the parts. Thus, a post-processing procedure should be applied during the topology optimization procedure. In addition, aggregated joints also appear. To overcome these difficulties, the concept of the joint dispersal (JD) constraint is developed here. The JD constraint subtracts the p-norm from the summation at the joint subdomain. With this JD constraint, up to one joint can appear at the joint subdomain. By imposing the JD constraint, it is possible to control the minimum distances between joints. The joint design formulation and the JD constraint are extended to plate structures and three-dimensional structures. To model the joint of a plate, the rotational degrees of freedom as well the translational degrees of freedom are considered in the joint formulation. To validate the concept of the JD constraint, several two-dimensional problems, two shell structure problems and one three-dimensional problem are considered, while the presented JD constraint is calculated using only the joint location and the topological density variable for the joint. This has some advantages over implementing other optimization methods such as composite delamination, fatigue, *etc.* For a future research topic, continuous-type joints are also one of the important subjects to consider. In addition, joint accessibility in three-dimensional problems should be considered.

Nomenclature

Ω	Analysis domain
Ω^i	The i-th subdomain ($i = 1, 2, \ldots, m$)
$\Omega^{i,j}$	Joint domain between Ω^i and Ω^j ($i, j = 1, 2, \ldots, m,\ i \neq j$)
$\Omega^{i,j,k}$	The k-th joint subdomains for the JD constraint in $\Omega^{i,j}$ ($k = 1, 2, \ldots, N^{i,j}$)
m	Number of subdomains
$m^{i,j}$	Number of joint subdomains for the JD constraint in $\Omega^{i,j}$
N^i	Number of topological design variables in subdomain Ω^i
$N^{i,j}$	Number of joints in joint domain $\Omega^{i,j}$
$N^{i,j,k}$	Number of joints in joint subdomain $\Omega^{i,j,k}$
V^i	Summation of volume in subdomain Ω^i
$V^i_{\max}$	Maximum volume constraint value in subdomain Ω^i
$V^{(i,j)}$:	Summation of joint design variables in joint domain $\Omega^{(i,j)}$
$V^{(i,j)}_{\max}$:	Maximum joint volume fraction in joint domain $\Omega^{(i,j)}$
$\varphi^{i,j}$	Joint dispersal constraint in joint domain $\Omega^{i,j}$
$\varphi^{i,j,k}$	Joint dispersal constraint in joint subdomain $\Omega^{i,j,k}$
δ	Distance value between two joints
$\delta_{\min}$	Minimum joint distance value for JD constraint
ϵ_1	Tolerance value for JD constraint
ϵ_2	Tolerance value for no-overlap constraint
$\mathbf{x}$	Design variables $\mathbf{x} = \gamma^i \cup \kappa^{i,j}$
γ^i	Topological design variables in subdomain Ω^i
$\kappa^{i,j}$	Joint design variables in joint domain $\Omega^{i,j}$
n	Penalization factor of the stiffness interpolation
$l^{i,j}_{\max}$	Stiffness value of the spring joint

$\alpha_{\max}^{i,j}$	Stiffness parameter of the spring joint
JD	Joint Dispersal
NSJ	Node Spring Joint
ESJ	Element Spring Joint
$T_{\max}^{i}$	The one-component constraint for a 3D problem in Ω^i
$\eta^{i,j}$	The no-overlap constraint for a 3D problem in $\Omega^{i,j}$

Disclosure statement

On behalf of all authors, the corresponding author states that there is no conflict of interest.

Data Available Statement

The data that support the findings of this study are available from the corresponding author, G.H.Yoon, upon reasonable request.

Funding

This work was supported by a National Research Foundation of Korea (NRF) grant funded by the Korea government (MSIT) [NRF-2019R1A2C2084974].

References

Ambrozkiewicz, Olaf, and Benedikt Kriegesmann. 2021. "Simultaneous Topology and Fastener Layout Optimization of Assemblies Considering Joint Failure." *International Journal for Numerical Methods in Engineering* 122 (1): 294–319.

Chickermane, Hemant, and Hae Chang Gea. 1996. "Design of Multi-Component Structural Systems for Optimal Layout Topology and Joint Locations." In *International Design Engineering Technical Conference & Computers and Information in Engineering Conference*, Vol. 97591, Paper No. 96-DETC/DAC-1467, V003T03A073. New York: ASME (American Society of Mechanical Engineers). doi:10.1115/96-DETC/DAC-1467.

Guirguis, David, Karim Hamza, Mohamed Aly, Hesham Hegazi, and Kazuhiro Saitou. 2015. "Multi-Objective Topology Optimization of Multi-Component Continuum Structures Via a Kriging-Interpolated Level Set Approach." *Structural and Multidisciplinary Optimization* 51 (3): 733–748.

Hur, Doe Young, Yuki Sato, Takayuki Yamada, Kazuhiro Izui, and Shinji Nishiwaki. 2019. *Level Set-Based Topology Optimization with Manufacturing Constraint with Manufacturing Directions via Fictitious Physical Model*. Paper No. AIAA 2019-1467. Reston, VA: AIAA (American Institute of Aeronautics and Astronautics). https://arc.aiaa.org/doi/abs/10.2514/6.2019-1467.

Jiang, Tao, and Mehran Chirehdast. 1996. "A Systems Approach to Structural Topology Optimization: Designing Optimal Connections." In *International Design Engineering Technical Conference & Computers and Information in Engineering Conference*, Vol. 97591, Paper No: 96-DETC/DAC-1474, V003T03A044. New York: ASME (American Society of Mechanical Engineers). doi:10.1115/96-DETC/DAC-1474.

Kang, Zhan, Yaguang Wang, and Yiqiang Wang. 2016. "Structural Topology Optimization with Minimum Distance Control of Multiphase Embedded Components by Level Set Method." *Computer Methods in Applied Mechanics and Engineering* 306: 299–318.

Kim, Cheolwoong, Hong Kyoung Seong, Il Yong Kim, and Jeonghoon Yoo. 2020. "Single Variable-Based Multi-Material Structural Optimization Considering Interface Behavior." *Computer Methods in Applied Mechanics and Engineering* 367: Article ID 113114. doi:10.1016/j.cma.2020.113114.

Langelaar, Matthijs. 2019. "Topology Optimization for Multi-Axis Machining." *Computer Methods in Applied Mechanics and Engineering* 351: 226–252.

Li, Quhao, Wenjiong Chen, Shutian Liu, and Liyong Tong. 2016. "Structural Topology Optimization Considering Connectivity Constraint." *Structural and Multidisciplinary Optimization* 54 (4): 971–984.

Li, Qing, Grant P. Steven, and Y. M. Xie. 2001. "Evolutionary Structural Optimization for Connection Topology Design of Multi-Component Systems." *Engineering Computations: International Journal for Computer-Aided Engineering* 18 (3-4): 460–479. https://www.ingentaconnect.com/content/mcb/182/2001/00000018/f0020003/art00006.

Liu, Pai, and Zhan Kang. 2018. "Integrated Topology Optimization of Multi-Component Structures Considering Connecting Interface Behavior." *Computer Methods in Applied Mechanics and Engineering* 341: 851–887.

Liu, Pai, Yangjun Luo, and Zhan Kang. 2016. "Multi-Material Topology Optimization Considering Interface Behavior Via XFEM and Level Set Method." *Computer Methods in Applied Mechanics and Engineering* 308: 113–133.

Liu, Pai, Litao Shi, and Zhan Kang. 2020. "Multi-Material Structural Topology Optimization Considering Material Interfacial Stress Constraints." *Computer Methods in Applied Mechanics and Engineering* 363: Article ID 112887. doi:10.1016/j.cma.2020.112887.

Luo, Yunfeng, Jingyu Hu, and Shutian Liu. 2021. "Self-Connected Multi-Domain Topology Optimization of Structures with Multiple Dissimilar Microstructures." *Structural and Multidisciplinary Optimization* 64 (1): 125–140.

Rajadhyaksha, Rahul. 2016. *A Definitive Guide to Design for Manufacturing Success—Spot Welding Design Guidelines*. 17th ed. Mumbai, India: Geometric Limited. https://dfmpro.com/wp-content/uploads/2016/02/DFM-Guidebook-Welding-Design-Guidelines-Issue-XVII.png.

Svanberg, Krister. 1987. "The Method of Moving Asymptotes—A New Method for Structural Optimization." *International Journal for Numerical Methods in Engineering* 24 (2): 359–373.

Thomas, Simon, Qing Li, and Grant Steven. 2020. "Topology Optimization for Periodic Multi-Component Structures with Stiffness and Frequency Criteria." *Structural and Multidisciplinary Optimization* 61: 2271–2289. doi:10.1007/s00158-019-02481-7.

Wang, Xuan, Kai Long, Van-Nam Hoang, and Ping Hu. 2018. "An Explicit Optimization Model for Integrated Layout Design of Planar Multi-Component Systems Using Moving Morphable Bars." *Computer Methods in Applied Mechanics and Engineering* 342: 46–70.

Woischwill, Christopher, and Il Yong Kim. 2018. "Multimaterial Multijoint Topology Optimization." *International Journal for Numerical Methods in Engineering* 115 (13): 1552–1579.

Yildiz, Ali R., and Kazuhiro Saitou. 2011. "Topology Synthesis of Multicomponent Structural Assemblies in Continuum Domains." *Journal of Mechanical Design* 133 (1). doi:10.1115/DETC2008-50037.

Yoon, Gil-Ho, Yoon Young Kim, Matthijs Langelaar, and Fred van Keulen. 2008. "Theoretical Aspects of the Internal Element Connectivity Parameterization Approach for Topology Optimization." *International Journal for Numerical Methods in Engineering* 76 (6): 775–797. doi:10.1002/nme.2342.

Zhang, Qiao, Weihong Zhang, Jihong Zhu, and Tong Gao. 2012. "Layout Optimization of Multi-Component Structures Under Static Loads and Random Excitations." *Engineering Structures* 43: 120–128. doi:10.1016/j.engstruct.2012.05.013.

Zhou, Hao, Junyuan Zhang, Yuqing Zhou, and Kazuhiro Saitou. 2019. "Multi-Component Topology Optimization for Die Casting (MTO-D)." *Structural and Multidisciplinary Optimization* 60 (6): 2265–2279.

Zhou, Yuqing, Tsuyoshi Nomura, and Kazuhiro Saitou. 2018. "Multi-Component Topology and Material Orientation Design of Composite Structures (MTO-C)." *Computer Methods in Applied Mechanics and Engineering* 342: 438–457.

Zhou, Yuqing, and Kazuhiro Saitou. 2018. "Gradient-Based Multi-Component Topology Optimization for Stamped Sheet Metal Assemblies (MTO-S)." *Structural and Multidisciplinary Optimization* 58 (1): 83–94.

Zhu, Ji-Hong, Huan-Huan Gao, Wei-Hong Zhang, and Ying Zhou. 2015. "A Multi-Point Constraints Based Integrated Layout and Topology Optimization Design of Multi-Component Systems." *Structural and Multidisciplinary Optimization* 51 (2): 397–407.

Zhu, J. H., and W. H. Zhang. 2010. "Integrated Layout Design of Supports and Structures." *Computer Methods in Applied Mechanics and Engineering* 199 (9-12): 557–569.

Zhu, Jihong, Weihong Zhang, and Pierre Beckers. 2009. "Integrated Layout Design of Multi-Component System." *International Journal for Numerical Methods in Engineering* 78 (6): 631–651.

Zhu, Jihong, Weihong Zhang, Pierre Beckers, Yuze Chen, and Zhongze Guo. 2008. "Simultaneous Design of Components Layout and Supporting Structures Using Coupled Shape and Topology Optimization Technique." *Structural and Multidisciplinary Optimization* 36 (1): 29–41.

Zhu, Ji-Hong, Wei-Hong Zhang, and Liang Xia. 2016. "Topology Optimization in Aircraft and Aerospace Structures Design." *Archives of Computational Methods in Engineering* 23 (4): 595–622.